Supporting Information

For

Atomic-Level Interfacial Engineering of Zr-In_2S_3/g-C_3N_4 Z-Scheme Heterojunction for Enhanced Photocatalytic CO_2 Reduction

Ahmed Uddin,[ab] Muhammad Bilal, [ab] Qingquan He, [ab] Jinchen Qian,[a] Jun Pan, [*a]

[a] Science and Education Integration College of Energy and Carbon Neutralization | College of Materials Science and Engineering | Zhejiang Provincial Key Laboratory of Clean Energy Conversion and Utilization | State Key Laboratory of Green Chemical Synthesis and Conversion, Zhejiang University of Technology, Hangzhou 310014, China.

[b] Moganshan Institute ZJUT, Kangqian District, Deqing 313200, China.

*Correspondence: panjun0123@zjut.edu.cn

Text Captions

Text S1. Materials

Text S2. Preparation of g-C_3N_4 nanosheet

Text S3. Preparation of Zirconium-doped In_2S_3 nanoparticles

Text S4. Preparation of Zr-In_2S_3/g-C_3N_4 heterojunctions

Text S5. Photocatalytic CO_2 reduction

Text S6. Density functional theory (DFT) calculations

Text S7. Characterizations

Text S8. Photoelectrochemical measurements

Fig. S1 Comparison of pore size distributions of Zr-In_2S_3, g-C_3N_4 and 20%Zr-In_2S_3/g-C_3N_4.

Fig. S2 SEM images of as prepared photocatalysts (a) g-C_3N_4 (b) Zr-In_2S_3 (c) Zr-In_2S_3/g-C_3N_4 (d) SEM-EDX profile.

Fig. S3. XPS survey of g-C_3N_4, Zr-In_2S_3 and Zr-In_2S_3/g-C3N_4 (a) Zr 3d (b)

Fig. S4 VBXPS peaks (a) Zr-In_2S_3 (b) g-C_3N_4.

Fig. S5 Photocatalytic and thermal-catalytic CO_2 conversion over 20%Zr-In_2S_3/g-C_3N_4.

Fig. S6 Mott-Schottky(M-S) plots (a) Zr-In_2S_3 (b) g-C_3N_4

Table. S1. The specific surface-area and pore-structure of as synthesized photocatalysts.

Table. S2 The binding energy values of Zr-In_2S_3, g-C_3N_4 and Zr-In_2S_3/g-C_3N_4.

Table. S3 The calculated value of band gap energy, valence band potential and conduction band potentials over Zr-In_2S_3 and g-C_3N_4 nanosheet.

Text. S1 Materials

Urea (CH_4N_2O) ≥99.0%, Dicyandiamide ($C_2H_4N_4$) ≥99%, Indium chloride ($InCl_3.4H_2O$) ≥98% thioacetamide (C_2H_5NS) ≥98% and Zirconium nitrate ($Zr(NO_3)_4$) ≥99%), were acquired from Sinopharm Chemical Reagent (Co., Ltd). Shanghai China and were used in this work as procured without any further purification.

Text. S2 Preparation of g-C_3N_4 nanosheet

g-C_3N_4 sheets were synthesized through a pyrolysis process involving urea and dicyandiamide. Specifically, 10 g of urea mixed with 2 g of dicyandiamide was placed in a covered alumina crucible. This mixture was then subjected to pyrolysis in a muffle furnace at 550 °C for 4 h, with a heating rate of 2 °C min^{-1} in air. After cooling to room temperature, the resulting yellow product was thoroughly washed with deionized (DI) water, rinsed with ethanol several times, and dried at 60 °C overnight.

Text. S3 Preparation of Zirconium-doped In_2S_3 nanoparticles

Zr-In_2S_3 nanoparticles were prepared via a hydrothermal procedure. Initially, 2.5 g of $InCl_3.4H_2O$ and 3 g of thioacetamide (C_2H_5NS) were dissolved in Ethylene glycol. Subsequently, 1.20 g of Zirconium nitrate ($Zr(NO_3)_4$) was added to the solution. After thorough stirring, the mixture was transferred to an autoclave and heated at 200 °C for 24 h. After cooling to room temperature, the Zr-In_2S_3 nanoparticles were separated by centrifugation, rinsed with ethanol and deionized water, and then dried under vacuum at 40 °C for 12 h.

Text. S4 Preparation of Zr-In_2S_3/g-C_3N_4 heterojunctions

Zr-In_2S_3/g-C_3N_4 heterojunctions were synthesized through a modified hydrothermal process. Initially, 200 mg of the as-prepared g-C_3N_4, 1.5 g of $InCl_3.4H_2O$, and 2.25 g of C_2H_5NS (TAA) were dissolved in ethylene glycol. Various amounts of $Zr(NO_3)_4$ (10%, 20%, and 30% by weight) were then added under magnetic stirring to achieve the desired Zr doping

concentrations. After vigorous stirring, the mixture was transferred into a Teflon-lined autoclave and heated at 200 °C for 24 h. The final products were annealed at 500 °C for 2 h, followed by washing several times with deionized water and ethanol, and dried for experimental usage. The obtained samples were denoted as (X)% Zr-doped In_2S_3/g-C_3N_4, where X represents the Zr weight percentage.

Text. S5 Photocatalytic CO_2 reduction

Photocatalytic CO_2 reduction experiments were carried out in a closed quartz reactor with a total volume of approximately 100 mL). A 15 mg sample of the synthesized photocatalyst was dispersed in deionized water and deposited onto a quartz substrate (2 × 2 cm^2) via drop-casting. The substrate was dried under ambient conditions and placed inside a reactor containing 5 mL of deionized water at the base. Prior to illumination, the reactor was purged with high-purity CO_2 (99.999%), saturated with water vapor, for 25 min to eliminate residual oxygen. The reaction temperature was stablilized at 25 °C using a circulating water cooling system. A 300 W Xe lamp (HF-GHX-XE-300, Shanghai Hefan Instrument Co., Ltd.) provided simulated solar illumination. The evolved gaseous products were analyzed in real time using an online gas chromatograph (GC-7890, Shandong Jinpu Analytical Instrument Co., Ltd.) equipped with flame ionization (FID) and thermal conductivity (TCD) detectors.

Text. S6 Density functional theory (DFT) calculations

DFT calculations were performed using the VASP software, employing the generalized Perdew–Burke–Ernzerhof (PBE) approximation and the projector augmented-wave (PAW) methodology. A Monkhorst-Pack k-point grid of 3×2 ×1 was applied for geometry optimizations of the unit cell, with a vacuum layer of approximately 10 Å inserted to prevent interactions between periodic images. The plane-wave energy cutoff was set to 500 eV. The

convergence criteria were set to 1×10^{-5} eV per atom for total energy and 0.02 eV·Å^{-1} for the maximum force.

Text. S7 Characterizations

Powder X-ray diffraction (XRD) patterns were verified using a PANalytical X'Pert PRO MPD diffractometer with Cu Kα radiation (λ = 1.5406 Å), operating at 40 kV and 30 mA. Scanning electron microscopy (SEM) images were acquired using a JSM-6700 microscope operated at an accelerating voltage of 5.0 kV. Transmission electron microscopy (TEM), high-resolution TEM (HR-TEM), high-angle annular dark-field scanning TEM (HAADF-STEM), energy-dispersive X-ray spectroscopy (EDS), and elemental mapping were accompanied using JEM-2100 and Tecnai G2 F20 U-TWIN microscopes, both operated at 200 kV. X-ray photoelectron spectroscopy (XPS) was carried out using an ESCALab 220i-XL spectrometer (VG Scientific) equipped with a 300 W Al Kα X-ray source. Diffuse reflectance spectra (DRS) were documented using a UV–Vis spectrophotometer (Cary 5000, Varian) with an integrating sphere, using $BaSO_4$ as the reference. Mott-Schottky analysis, electrochemical impedance spectroscopy (EIS), and time-resolved photocurrent measurements were performed on a CH Instruments electrochemical workstation in a standard three electrode configuration, with the sample coated FTO glass as the working electrode, a Pt foil as the counter electrode, and Ag/AgCl as the reference electrode, using 0.1 M Na_2SO_4 as the electrolyte. Time-resolved and steady state photoluminescence (PL) spectra were documented using a NanoLOG-TCSPC spectrofluorometer (HORIBA Jobin Yvon) under 270 nm excitation.

Text. S8 Photoelectrochemical measurements

Electrochemical impedance spectroscopy (EIS), and transient photocurrent response measurements were carried out using a CHI 660E electrochemical workstation in a standard three-electrode setup. The working electrode was prepared by coating the synthesized

photocatalyst onto indium tin oxide (ITO) glass substrates, with a platinum wire and an Ag/AgCl electrode (saturated KCl) serving as the counter and reference electrodes, respectively. For the photocurrent measurements, three consecutive light on/off cycles were conducted. To fabricate the working electrode, 5 mg of the catalyst powder was dispersed in a solution containing 4 mL of ethanol and 15 μL of Nafion to form a uniform slurry. This slurry was evenly applied to a 1 × 1 cm^2 area of the ITO substrate and then dried at 40 °C in an oven for 6 hours.

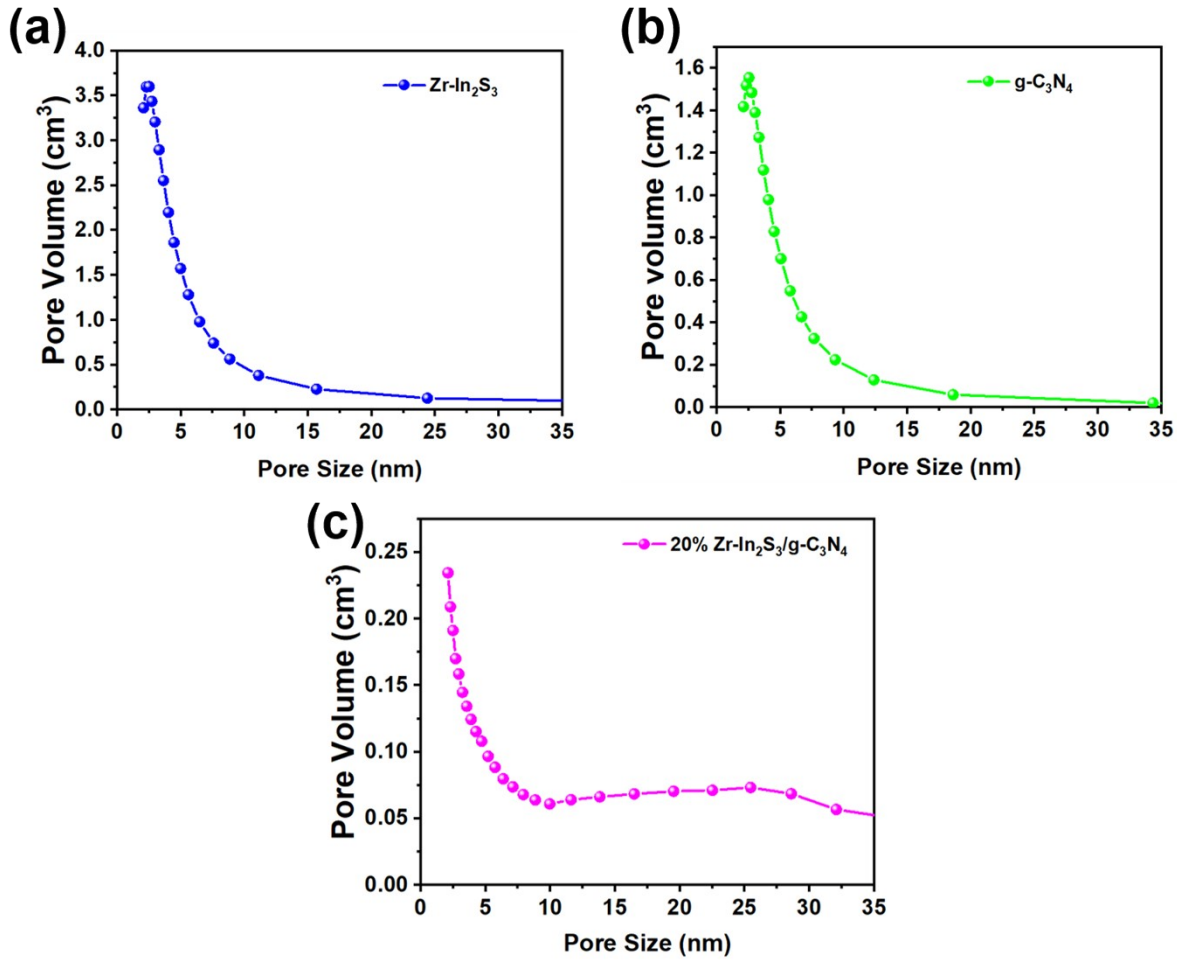

Fig. S1. Comparison of pore size distributions of (a) Zr-In_2S_3, (b) g-C_3N_4, and (c) 20%Zr-In_2S_3/g-C_3N_4.

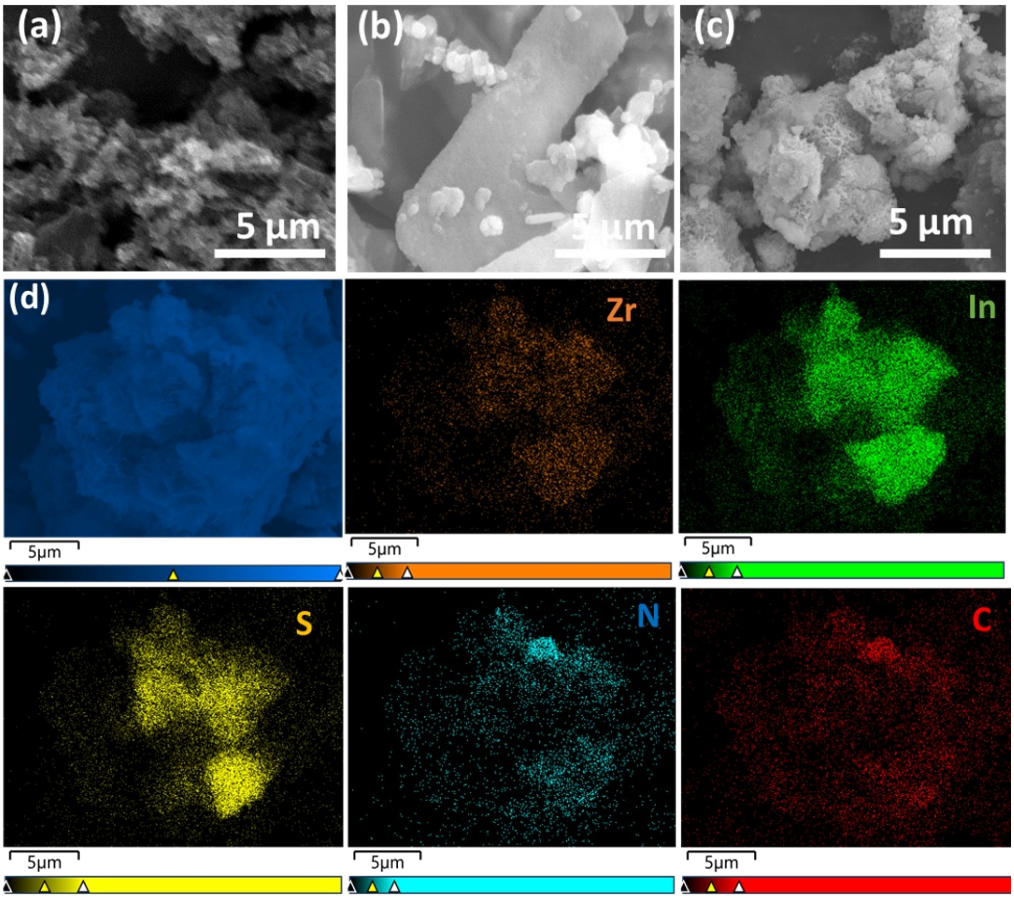

Fig. S2. Scanning electron microscopy (SEM) image (a) g-C_3N_4 (b) Zr-In_2S_3 and (c) Zr-In_2S_3/g-C_3N_4 (d) energy dispersive X-ray spectroscopy (EDX) elemental mapping of Zr, In, S, N and C elements in Zr-In_2S_3/g-C_3N_4 heterojunction.

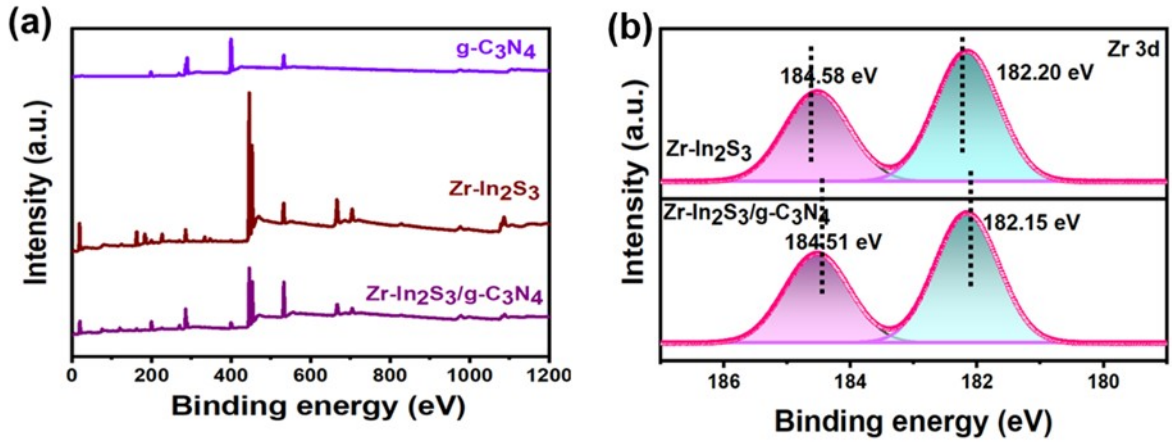

Fig. S3. XPS survey of Zr-In_2S_3, g-C_3N_4, and Zr-In_2S_3/g-C_3N_4 (a) XPS spectra Zr 3d (b)

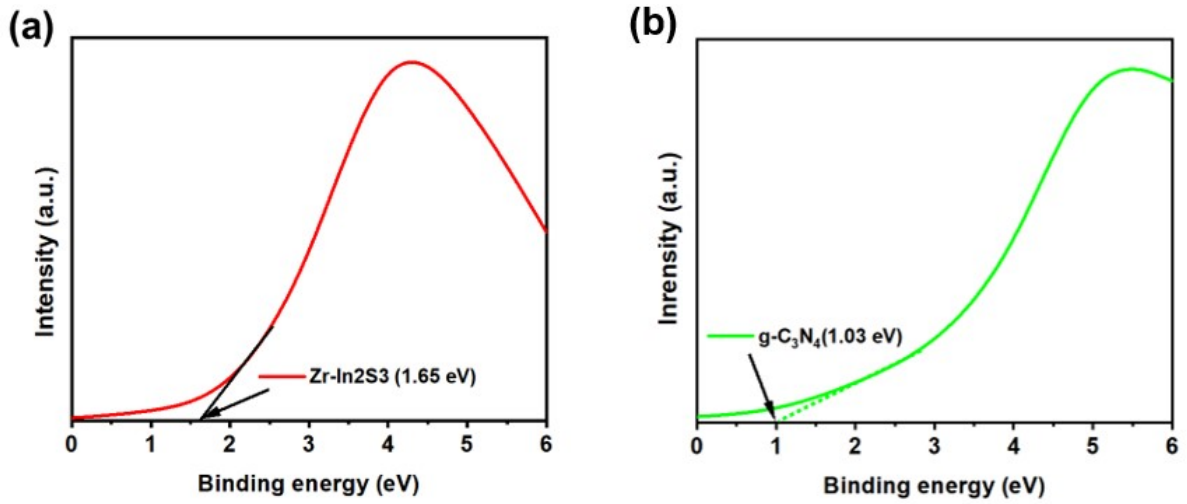

Fig. S4. VBXPS peaks (a) Zr-In_2S_3 (b) g-C_3N_4

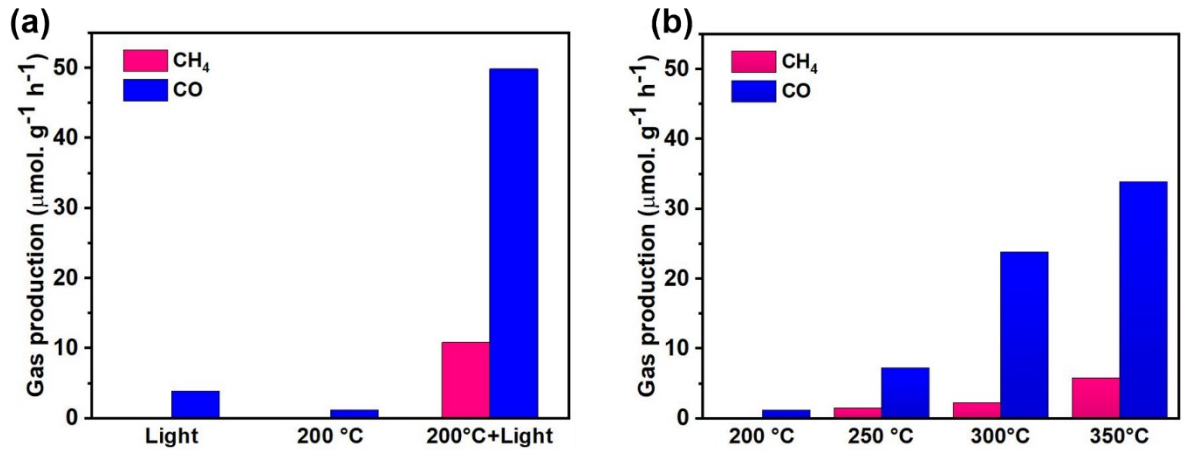

Fig. S5. Photocatalytic and thermal-catalytic CO_2 conversion over 20%Zr-In_2S_3/g-C_3N_4.

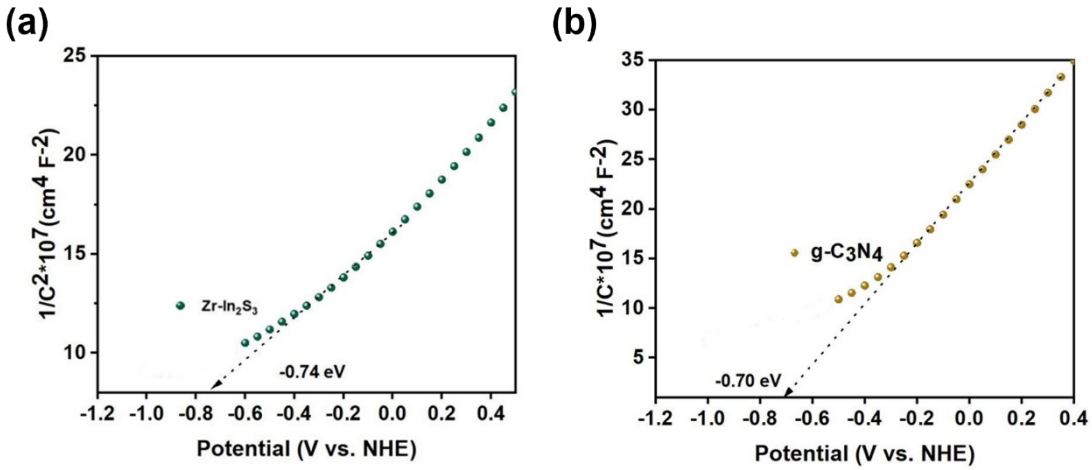

Fig. S6. Mott-Schottky (M-S) plots (a) Zr-In_2S_3 (b) g-C_3N_4.

Table. S1. The specific surface-area and pore-structure of as synthesized photocatalysts.

Samples	Pore Volume (cm^3/g)	Pore Size (nm)	Specific Surface Area (m^2/g
Zr-In_2S_3	0.22	2.49	34.19
g-C_3N_4	0.08	2.52	13.29
20%Zr-In_2S_3/g-C_3N_4	0.39	2.10	73.62

Table. S2 The binding energy values of Zr-In_2S_3, g-C_3N_4 and Zr-In_2S_3/g-C_3N_4

Peak-Name	Zr-In_2S_3/peak value (eV)	g-C_3N_4/peak value (eV)	Zr-In_2S_3/g-C_3N_4/peak value (eV)
C 1s		288.49	288.78
C 1s		284.78	285.01
N 1s		400.22	399.85
N 1s		398.90	398.62
Zr 3d	184.58	-	184.51
Zr 3d	182.20	-	182.15
In 3d	452.71		452.34
In 3d	445.15		444.77
S 2p	161.38		162.40
S 2p	162.53		162.60

Table. S3 The calculated value of band gap energy, valence band potential and conduction band potentials over Zr-In_2S_3 and g-C_3N_4 nanosheet.

Photocatalysts	Band gap energy (eV)	Valence band potential (eV)	Conduction band potential (eV)
Zr-In_2S_3	2.75	1.65	-1.1
g-C_3N_4	2.33	1.03	-1.3

Table. S4. The calculated PL lifetimes (τ_1 and τ_2) and their corresponding amplitude factors (A_1 and A_2)

Samples	τ_1 and τ_2	A_1 and A_2	r_{avg}
Zr-In_2S_3	0.22	2.97	3.92
g-C_3N_4	0.08	3.32	3.90
20%Zr-In_2S_3/g-C_3N_4	0.39	28.60	4.87